Alias-Free Subband Adaptive Filtering With Critical Sampling

SangGyun Kim, *Student Member, IEEE*, Chang D. Yoo, *Member, IEEE*, and Truong Q. Nguyen, *Fellow, IEEE*

***Abstract*—To overcome the limitations of a conventional fullband adaptive filtering, various subband adaptive filtering (SAF) structures have been proposed. Properly designed, an SAF will converge faster at a lower computational cost than a fullband structure. However, its design should consider the following two facts: the interband aliasing introduced by the downsampling process degrades its performance, and the filter bank in the SAF introduces additional computational overhead and system delay. In this paper, to fully exploit the benefits of using an SAF, an almost alias-free SAF structure with critical sampling is proposed. The interband alising is removed from the subband signal by isolating the aliasing using a bandwidth-increased analysis filter. Computer simulations show that the proposed structure converges faster than both an equivalent fullband structure at lower computational complexity and recently proposed SAF structures for a colored input.**

***Index Terms*—Adaptive filtering, interband aliasing, LMS algorithm, multirate signal processing, subband adaptive filtering.**

I. Introduction

An adaptive filter is often employed in an environment of unknown statistics for various purposes such as system identification, inverse modelling for channel equalization, adaptive prediction, and interference cancelling. Knowing nothing about the environment, the filter is initially set to an arbitrary condition and updated in a step-by-step manner toward an optimum filter setting. For updating, the least mean-square (LMS) algorithm is often used for its simplicity and robust performance [1]. However, the LMS algorithm exhibits slow convergence when used with an ill-conditioned input such as speech and requires a high computational cost, especially when the system to be identified has a long impulse response [2]. One promising method that improves the performance and reduces the computational cost is subband adaptive filtering (SAF), in which the input is decomposed into a number of subband signals, and the adaptive filtering is performed on each subband [3]–[10]. It has the potential for a faster convergence and a lower computational complexity than a fullband structure. However, a subband structure suffers from two deficiencies. First, the interband aliasing that is introduced by the downsampling process required in reducing the data rate is unavoidable and degrades the performance. Second, the filter bank introduces additional computation and system delay. For these reasons, various SAF structures were proposed. In [3], an SAF using nonoverlapping subbands was proposed to mitigate the interband aliasing; however, it leads to output distortion in the form of spectral gaps that are very large. In [4] and [5], cross-adaptive filters between the subbands were used to compensate for the interband aliasing. Their use requires additional computational cost, and despite the increased computational complexity, its convergence is slow. In [6], an SAF using auxiliary channels was proposed to avoid both interband aliasing and spectral gaps; however, this results in increased complexity. In [7], [8], an oversampled filter bank was used to reduce interband aliasing; however, its computational complexity was increased, and it has been found to have slow convergence [2]. In [9], [10], subband structures that can exactly model an finite-impulse-response (FIR) system were proposed. In [9], a subband structure based on the polyphase decomposition of an FIR system to be adaptively modelled was proposed; however, its computational complexity is similar to that of the fullband structure. In [10], a subband structure proposed in [11] was used to exactly model an arbitrary FIR system. This structure requires additional computation for adaptively filtering the overlappings between adjacent subbands.

In this paper, a critically sampled SAF structure that is almost alias-free is proposed to reap all the benefits of using an SAF. Since the proposed SAF is performed using subbands that is almost alias-free, there is little interband aliasing error at the output. In each subband, the interband aliasing is obtained using a bandwidth-increased linear-phase FIR analysis filter, whose passband has almost-unit magnitude response in the subband interval, and is then subtracted from the subband signal. This aliasing cancellation procedure, however, causes the spectral dips of the subband signals. These spectral dips can be reduced by using a simple FIR filter.

The paper is organized as follows. Section II discusses the reason why the interband aliasing yields large mean-squared error (MSE). Section III proposes a critically sampled SAF structure that is almost alias-free. Section IV represents the improvement of the spectral flatness of the almost alias-free subband signals. Section V presents the design procedures of the bandwidth-increased analysis filters to obtain the interband aliasing. Section VI represents the computational complexity of the proposed algorithm. Section VII compares simulation results of the proposed SAF structure to those of the equivalent fullband structure and recently proposed SAF structures, and Section VIII concludes the paper.

Manuscript received July 3, 2006; revised September 24, 2007. The associate editor coordinating the review of this manuscript and approving it for publication was Dr. Kostas Berberidis. This work was supported by Grant No. R01-2007-000-20949-0 from the Basic Research Program of the Korea Science and Engineering Foundation.

S. G. Kim and C. D. Yoo are with the Division of Electrical Engineering, School of Electrical Engineering and Computer Science, Korea Advanced Institute of Science and Technology, Daejeon 305-701, Korea (e-mail: zom@eeinfo.kaist.ac.kr; cdyoo@ee.kaist.ac.kr).

T. Q. Nguyen is with the Department of Electrical and Computer Engineering, University of California, San Diego, La Jolla, CA 92093-0407 USA (e-mail: nguyent@ece.ucsd.edu).

Digital Object Identifier 10.1109/TSP.2007.912262

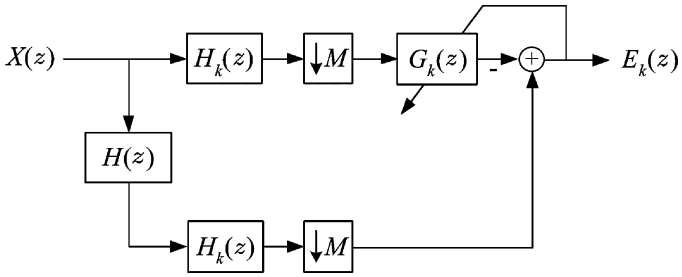

Fig. 1. Block diagram of the adaptive filtering in the kth subband. $X(z)$, $H(z)$, $H_k(z)$, $G_k(z)$, and $E_k(z)$ represent the z-transforms of input, unknown system, the kth analysis filter, the kth adaptive filter, and the kth error signal for $k = 0, 1, \ldots, M-1$, respectively.

II. SAF With Critical Sampling

In SAF, signals are decomposed into a number of subband signals using an analysis filter bank, and the adaptive filtering is performed on each subband. The result in each subband is combined into an output using a synthesis filter bank. For a critically sampled SAF with M subbands, the kth subband error $E_k(z)$, shown in Fig. 1, is given as

$$\begin{aligned} E_k(z) = \frac{1}{M}\sum_{i=0}^{M-1} & H_k\left(z^{1/M}W_M^i\right) H\left(z^{1/M}W_M^i\right) \\ & \times X\left(z^{1/M}W_M^i\right) - \frac{1}{M}G_k(z) \\ & \times \sum_{i=0}^{M-1} H_k\left(z^{1/M}W_M^i\right) X\left(z^{1/M}W_M^i\right) \end{aligned} \tag{1}$$

where $X(z)$, $H(z)$, $H_k(z)$, and $G_k(z)$ represent the z-transforms of input signal, unknown system, the kth analysis filter, and the kth adaptive filter for $k = 0, 1, \ldots, M-1$, respectively. Note $W_M^i = e^{-j2\pi i/M}$, and the kth analysis filter $H_k(z)$ is a bandpass filter, whose passband is $k\pi/M \le \omega \le (k+1)\pi/M$. Equation (1) can be rewritten as

$$\begin{aligned} M \cdot E_k(z) = & \left[H(z^{1/M}) - G_k(z)\right] H_k(z^{1/M}) X(z^{1/M}) \\ & + \left[H(z^{1/M}W_M^k) - G_k(z)\right] \\ & \times H_k\left(z^{1/M}W_M^k\right) X\left(z^{1/M}W_M^k\right) \\ & + \left[H\left(z^{1/M}W_M^{k+1}\right) - G_k(z)\right] \\ & \times H_k\left(z^{1/M}W_M^{k+1}\right) X\left(z^{1/M}W_M^{k+1}\right) + \xi_k(z) \end{aligned} \tag{2}$$

where

$$\begin{aligned} \xi_k(z) = & \sum_{\substack{i=1 \\ i\neq k,k+1}}^{M-1} H_k\left(z^{1/M}W_M^i\right) H\left(z^{1/M}W_M^i\right) \\ & \times X\left(z^{1/M}W_M^i\right) - G_k(z) \\ & \times \sum_{\substack{i=1 \\ i\neq k,k+1}}^{M-1} H_k\left(z^{1/M}W_M^i\right) X\left(z^{1/M}W_M^i\right). \end{aligned} \tag{3}$$

When the filter bank is real-valued, the terms $H_k(z^{1/M}W_M^k)$ and $H_k(z^{1/M}W_M^{k+1})$ are adjacent to $H_k(z^{1/M})$ as shown by their magnitude responses in Fig. 2, and when $H_k(z)$ is designed with high enough stopband attenuation, $\xi_k(z)$ is approximately zero [12].

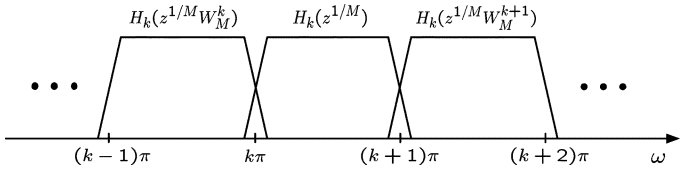

Fig. 2. Magnitude responses of $H_k(z^{1/M})$ and its adjacent terms $H_k\left(z^{1/M}W_M^k\right)$ and $H_k\left(z^{1/M}W_M^{k+1}\right)$.

The second and third terms on the right-hand side of (2) are the errors introduced by interband aliasing due to the overlappings between $H_k\left(z^{1/M}W_M^k\right)$ and $H_k(z^{1/M})$ and between $H_k\left(z^{1/M}W_M^{k+1}\right)$ and $H_k(z^{1/M})$. In order to reduce $|E_k(z)|$ to a value close to zero, the adaptive filter $G_k(z)$ has to match the two different frequency responses, that is, both $H\left(z^{1/M}W_M^k\right)$ and $H(z^{1/M})$ which have considerable overlap and both $H\left(z^{1/M}W_M^{k+1}\right)$ and $H(z^{1/M})$ which also have considerable overlap between them. Of course, this is impossible. These mismatches result in a large $|E_k(z)|$ around $\omega = k\pi$ and $(k+1)\pi$ even after convergence, therefore, the SAF with critical sampling has a large MSE at the output.

III. Alias-Free SAF With Critical Sampling

The interband aliasing is a major bottleneck in using SAF, and several methods for reducing the interband aliasing have been proposed [3]–[10]. In this paper, critically sampled SAF that is almost alias-free is proposed. The interband aliasing components are caused by downsampling the signal which has passed through a nonideal analysis filter: the downsampling process is essential in almost all multirate signal processing for making the overall data rate nearly equivalent to that of the input. Fig. 3 shows the magnitude responses $X_k(e^{j\omega})$ of the signal that has passed through the kth analysis filter, whose transition bandwidth is ω_δ/M, and its downsampled version $X_k^d(e^{j\omega})$ for $k = 0, 1, \ldots, M-1$.

Henceforth, only the frequency interval of $k\pi \le \omega \le (k+1)\pi$ will be considered, since the frequency responses in the other intervals are just the frequency-shifted and the frequency-flipped versions of the response in this interval. As shown in Fig. 3(b), the frequency interval of $k\pi \le \omega < (k+1)\pi$ is divided into three subintervals: $\Omega_1 = \{\omega | k\pi \le \omega < k\pi + \omega_\delta\}$, where the first and second terms on the right-hand side of (2) coexist, $\Omega_2 = \{\omega | k\pi + \omega_\delta \le \omega < (k+1)\pi - \omega_\delta\}$, where only the first term exists, and $\Omega_3 = \{\omega | (k+1)\pi - \omega_\delta \le \omega \le (k+1)\pi\}$, where the first and third terms coexist. As shown in Fig. 3(b), the error signal $E_k(e^{j\omega})$ of the kth subband is analyzed according to the subintervals as follows. For $\omega \in \Omega_1$, the error $E_k(e^{j\omega})$ can be approximated as

$$\begin{aligned} M \cdot E_k(e^{j\omega}) \approx & \left[H(e^{j\omega/M}) - G_k(e^{j\omega})\right] \\ & \times H_k(e^{j\omega/M}) X(e^{j\omega/M}) \\ & + \left[H(e^{j(\omega-2\pi k)/M}) - G_k(e^{j\omega})\right] \\ & \times H_k(e^{j(\omega-2\pi k)/M}) X(e^{j(\omega-2\pi k)/M}). \end{aligned} \tag{4}$$

For $\omega \in \Omega_2$, it can be approximated as

$$M \cdot E_k(e^{j\omega}) \approx \left[H(e^{j\omega/M}) - G_k(e^{j\omega})\right] H_k(e^{j\omega/M}) X(e^{j\omega/M}). \tag{5}$$

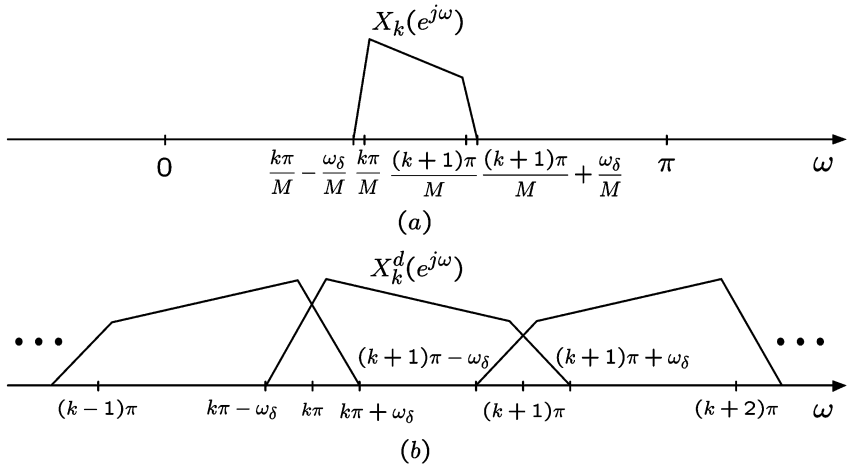

Fig. 3. Magnitude responses of the signals in the kth subband. (a) Output of the kth analysis filter. (b) Its downsampled version.

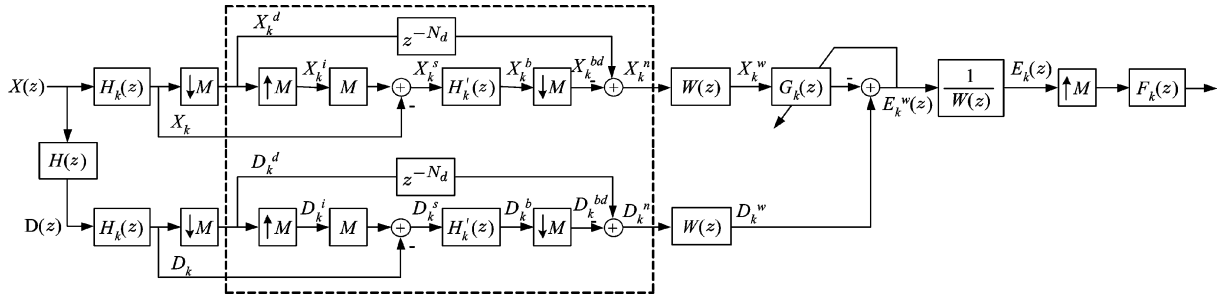

Fig. 4. Alias-free SAF structure with critical sampling in the kth subband. The dashed box is inserted into the SAF structure of Fig. 1 except $W(e^{j\omega})$ and $1/W(e^{j\omega})$ to cancel the interband aliasing. $H_k'(e^{j\omega})$, $X_k^b(e^{j\omega})$, $X_k^n(e^{j\omega})$, $W(e^{j\omega})$, $X_k^w(e^{j\omega})$, and $F_k(e^{j\omega})$ represent the linear-phase bandwidth-increased analysis filter, the extracted interband aliasing component, the almost alias-free subband input with the spectral dips, the minimum-phase filter for the spectral flatness of the subband input, the almost alias-free subband input with the flat spectrum, and the synthesis filter in the kth subband, respectively. The same analysis is also applied to $D_k(e^{j\omega})$, which is the kth subband signal of the desired signal $D(e^{j\omega})$, and thus the almost alias-free subband desired signal with the flat spectrum $D_k^w(e^{j\omega})$ is obtained. $X_k^w(e^{j\omega})$ and $D_k^w(e^{j\omega})$ are used as an input and a desired signal of the adaptive filter $G_k(e^{j\omega})$, respectively. The output $E_k^w(e^{j\omega})$ passes through the inverse filter $1/W(e^{j\omega})$, and $E_k(e^{j\omega})$ is finally obtained.

Finally, for $\omega \in \Omega_3$, it can be approximated as

$$\begin{aligned} M \cdot E_k(e^{j\omega}) \approx & [H(e^{j\omega/M}) - G_k(e^{j\omega})] \\ & \times H_k(e^{j\omega/M}) X(e^{j\omega/M}) \\ & + \left[H(e^{j(\omega-2\pi(k+1))/M}) - G_k(e^{j\omega})\right] \\ & \times H_k(e^{j(\omega-2\pi(k+1))/M}) X(e^{j(\omega-2\pi(k+1))/M}). \end{aligned} \tag{6}$$

From (4) and (6), the kth adaptive filter $G_k(e^{j\omega})$ has to match the desired response $H(e^{j\omega/M})$ while simultaneously matching the aliased response $H(e^{j(\omega-2\pi k)/M})$ at $\omega \in \Omega_1$ and the aliased response $H(e^{j(\omega-2\pi(k+1))/M})$ at $\omega \in \Omega_3$ in order to make $\left|E_k(e^{j\omega})\right|$ zero. This is impossible.

In this paper, a novel SAF structure that approximately eliminates the interband aliasing terms is proposed. The kth subband portion of the proposed SAF structure is shown in Fig. 4.

In Fig. 4, $H_k'(e^{j\omega})$ is a linear-phase bandwidth-increased analysis filter of the order $2MN_d$ where N_d is an integer and determines the order of $H_k'(e^{j\omega})$, whose magnitude response is almost one from $k\pi/M$ to $(k+1)\pi/M$, and $F_k(e^{j\omega})$ is the kth synthesis filter for $k = 0, 1, \ldots, M-1$. As shown in Fig. 4, the interband aliasing component $X_k^b(e^{j\omega})$ is extracted using the bandwidth-increased analysis filter $H_k'(e^{j\omega})$ and then its decimated version $X_k^{bd}(e^{j\omega})$ is subtracted from the subband signal $X_k^d(e^{j\omega})$ to obtain the almost alias-free $X_k^n(e^{j\omega})$. The spectral dips of $X_k^n(e^{j\omega})$ are reduced using a minimum-phase filter $W(e^{j\omega})$, and the result $X_k^w(e^{j\omega})$ is used as an input of the adaptive filter $G_k(e^{j\omega})$. The same analysis is also applied to $D_k(e^{j\omega})$, which is the kth subband signal of the desired signal $D(e^{j\omega})$, and thus the almost alias-free subband desired signal with flat spectrum $D_k^w(e^{j\omega})$ is obtained and used as a desired signal of the adaptive filter $G_k(e^{j\omega})$. The output of $G_k(e^{j\omega})$, $E_k^w(e^{j\omega})$, passes through $1/W(e^{j\omega})$ to negate the effect of $W(e^{j\omega})$, and then $E_k(e^{j\omega})$ is obtained.

Figs. 5 and 6 sequentially explain how the interband aliasing is eliminated from $X_k^d(e^{j\omega})$ in more detail.

In the kth subband, $X_k^d(e^{j\omega})$ is given as

$$\begin{aligned} X_k^d(e^{j\omega}) &= \frac{1}{M}\sum_{i=0}^{M-1} H_k(e^{j(\omega-2\pi i)/M}) X(e^{j(\omega-2\pi i)/M}) \\ &= \frac{1}{M}\Bigg[H_k(e^{j\omega/M}) X(e^{j\omega/M}) \\ &\quad + H_k(e^{j(\omega-2\pi k)/M}) X(e^{j(\omega-2\pi k)/M}) \\ &\quad + H_k(e^{j(\omega-2\pi(k+1))/M}) \\ &\quad \times X(e^{j(\omega-2\pi(k+1))/M})\Bigg] + \epsilon_k(e^{j\omega}) \end{aligned} \tag{7}$$

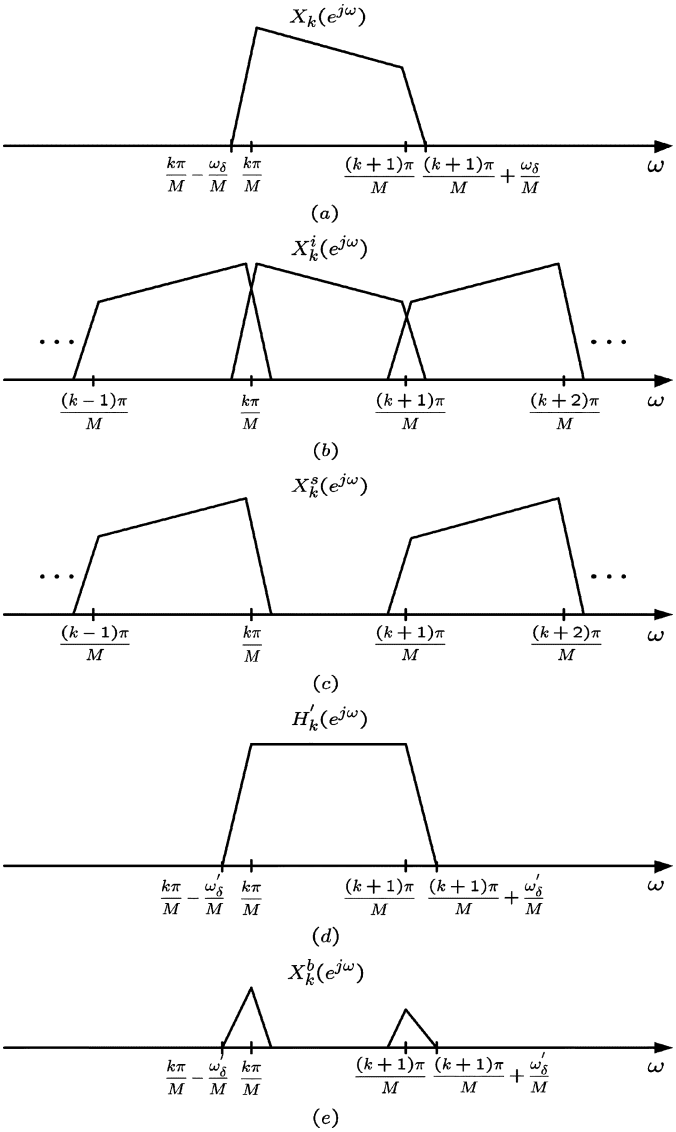

Fig. 5. Magnitude responses of the signals of the proposed SAF structure. (a) Output signal of the kth analysis filter. (b) Interpolated version of $X_k^d(e^{j\omega})$. (c) Resulting signal after subtracting $X_k(e^{j\omega})$ from $M\cdot X_k^i(e^{j\omega})$. (d) kth bandwidth-increased analysis filter. (e) Extracted interband aliasing component.

where

$$\epsilon_k(e^{j\omega}) = \frac{1}{M}\sum_{\substack{i=1\\ i\neq k,k+1}}^{M-1} H_k(e^{j(\omega-2\pi i)/M})X(e^{j(\omega-2\pi i)/M}). \tag{8}$$

The analysis filters $H_k(e^{j\omega})$ can be designed such that the overlapping $\epsilon_k(e^{j\omega})$ between nonadjacent terms can be much smaller than the overlapping between adjacent ones and thus negligible for $k=0,1,\ldots,M-1$. In order to eliminate the aliasing term from $X_k^d(e^{j\omega})$, the aliasing components should be obtained first. To do so, the output signal of the analysis filter $X_k(e^{j\omega})$ in Fig. 5(a) is subtracted from the interpolated signal $X_k^i(e^{j\omega})$ in Fig. 5(b), and the result is $X_k^s(e^{j\omega})$ as shown in Fig. 5(c). The mathematical expression of the result is given as

$$\begin{aligned} X_k^s(e^{j\omega}) &= M\cdot X_k^i(e^{j\omega}) - X_k(e^{j\omega}) \\ &= \sum_{i=0}^{M-1} X_k(e^{j(\omega-2\pi i/M)}) - X_k(e^{j\omega}) \\ &= \sum_{i=1}^{M-1} X_k(e^{j(\omega-2\pi i/M)}) \end{aligned} \tag{9}$$

where M is multiplied to $X_k^i(e^{j\omega})$, since the amplitude of $X_k(e^{j\omega})$ is reduced by M during the downsampling procedure. As shown in Fig. 5(c), $X_k^s(e^{j\omega})$ includes only the interband aliasing components in $k\pi/M \le \omega \le (k+1)\pi/M$. The interband aliasing components are extracted by passing $X_k^s(e^{j\omega})$ through the kth bandwidth-increased analysis filter $H_k'(e^{j\omega})$, whose magnitude response is almost-flat from $k\pi/M$ to $(k+1)\pi/M$ as shown in Fig. 5(d); this is the reason why the term "bandwidth-increased" is used for $H_k'(e^{j\omega})$. In general, the frequency interval where the magnitude response of the passband of the filter bank is almost-flat is narrower than that of $H_k'(e^{j\omega})$ for a perfect reconstruction (PR) of the filter bank. However, since $H_k'(e^{j\omega})$ is not an ideal filter and therefore has the transition intervals in $k\pi/M-\omega_\delta'/M \le \omega \le k\pi/M$ and $(k+1)\pi/M \le \omega \le (k+1)\pi/M+\omega_\delta'/M$, the output of the filter $H_k'(e^{j\omega})$, $X_k^b(e^{j\omega})$, contains the unwanted signals in the transition intervals, which will cause another interband aliasing components after the downsampling procedure. These aliasing components are analyzed in Fig. 6. In $0 \le \omega \le \pi$, $H_k'(e^{j\omega})$ overlaps predominantly with $X_k(e^{j(\omega-2\pi i/M)})$ when $i=k$ and $i=k+1$, thus $X_k^b(e^{j\omega})$ is given as

$$\begin{aligned} X_k^b(e^{j\omega}) &= H_k'(e^{j\omega})X_k^s(e^{j\omega}) \\ &= H_k'(e^{j\omega}) \\ &\quad\times\Big[X_k(e^{j(\omega-2\pi k/M)}) + X_k(e^{j(\omega-2\pi(k+1)/M)}) \\ &\quad + M\cdot\epsilon_k(e^{jM\omega})\Big] \end{aligned} \tag{10}$$

which is shown in Fig. 5(e). In $-\pi \le \omega \le 0$, $H_k'(e^{j\omega})$ overlaps predominantly with $X_k(e^{j(\omega-2\pi i/M)})$ when $i=-k$ (or $M-k$) and $i=-k-1$ (or $M-k-1$), thus $X_k^b(e^{j\omega})$ is given by

$$\begin{aligned} X_k^b(e^{j\omega}) = H_k'(e^{j\omega})\Big[&X_k(e^{j(\omega+2\pi k/M)}) \\ &+X_k(e^{j(\omega+2\pi(k+1)/M)}) + M\cdot\epsilon_k'(e^{jM\omega})\Big] \end{aligned} \tag{11}$$

where

$$\begin{aligned} M\cdot\epsilon_k'(e^{jM\omega}) = \sum_{\substack{i=1\\ i\neq M-k,M-k-1}}^{M-1} &H_k(e^{j(\omega-2\pi i)/M}) \\ &\times X(e^{j(\omega-2\pi i)/M}). \end{aligned} \tag{12}$$

After downsampling $X_k^b(e^{j\omega})$, an unwanted interband aliasing occurs due to the overlapping between $X_k^b(e^{j\omega})$ in $-\pi \le \omega \le 0$ represented in (11) and $X_k^b(e^{j\omega})$ in $0 \le \omega \le \pi$ represented

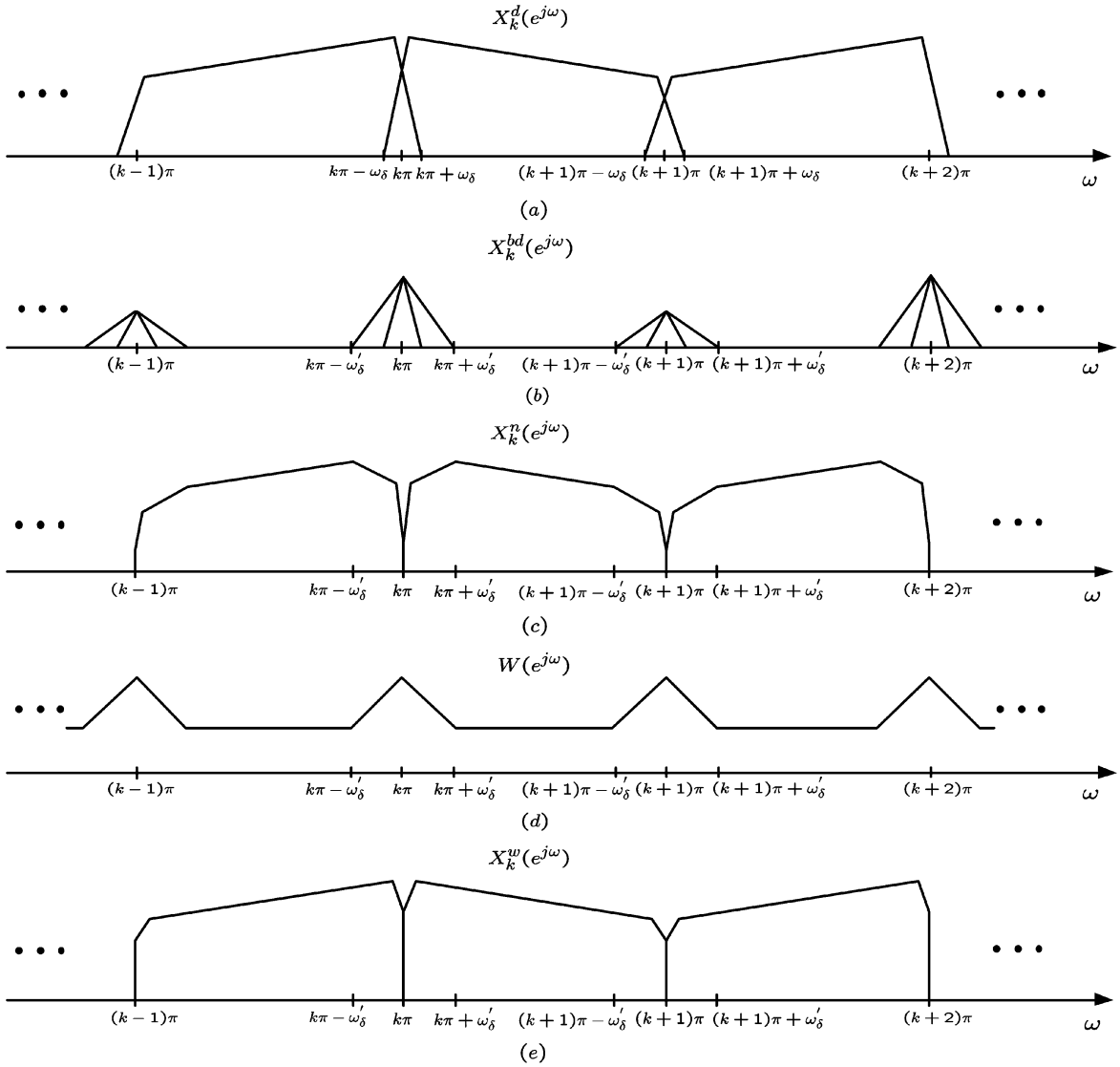

Fig. 6. Magnitude responses of the signals of the proposed SAF structure. (a) Subband input with interband aliasing. (b) Downsampled version of the extracted interband aliasing component. (c) Almost alias-free subband input. (d) Filter for the spectral flatness of the almost alias-free subband signal. (e) Almost alias-free subband input with the flat spectrum.

in (10). The downsampled interband aliasing component $X_k^{bd}(e^{j\omega})$ of Fig. 6(b) is given as

$$\begin{aligned} M\cdot X_k^{bd}(e^{j\omega}) &= \sum_{l=0}^{M-1} H_k'(e^{j(\omega-2\pi l)/M}) X_k^s(e^{j(\omega-2\pi l)/M}) \\ &\approx H_k'(e^{j\omega/M}) \\ &\quad\times \Big[X_k(e^{j(\omega-2\pi k)/M}) \\ &\qquad + X_k(e^{j(\omega-2\pi(k+1))/M})\Big] \\ &\quad + H_k'(e^{j(\omega-2\pi k)/M}) X_k(e^{j\omega/M}) \\ &\quad + H_k'(e^{j(\omega-2\pi(k+1))/M}) X_k(e^{j\omega/M}). \end{aligned} \tag{13}$$

The first term of the right-hand side of the approximation in (13) is the extracted interband aliasing component derived from $X_k^b(e^{j\omega})$ in $0\le\omega\le\pi$. The second and the third terms of the right-hand side of the approximation are the unwanted interband aliasing components, which came from $X_k^b(e^{j\omega})$ in $-\pi\le\omega\le 0$. All the other terms are negligible except the three terms mentioned above.

As shown in Fig. 4, the kth almost alias-free subband input signal $X_k^n(e^{j\omega})$ is obtained as

$$X_k^n(e^{j\omega}) = e^{-jN_d\omega} X_k^d(e^{j\omega}) - X_k^{bd}(e^{j\omega}) \tag{14}$$

where N_d is one Mth of the delay introduced by $H_k'(e^{j\omega})$. By inserting (7) and (13) into (14) and then representing $H_k'(e^{j\omega/M})$ as $e^{-jN_d\omega}$ in $k\pi\le\omega\le(k+1)\pi$, $X_k^n(e^{j\omega})$ is given by

$$\begin{aligned} &M\cdot X_k^n(e^{j\omega}) \\ &\quad\approx e^{-jN_d\omega}\Big[X_k(e^{j\omega/M}) + X_k(e^{j(\omega-2\pi k)/M}) \\ &\qquad + X_k(e^{j(\omega-2\pi(k+1))/M})\Big] \\ &\qquad - H_k'(e^{j\omega/M}) \\ &\qquad\times [X_k(e^{j(\omega-2\pi k)/M}) + X_k(e^{j(\omega-2\pi(k+1))/M})] \\ &\qquad - [H_k'(e^{j(\omega-2\pi k)/M}) + H_k'(e^{j(\omega-2\pi(k+1))/M})] \\ &\qquad\times X_k(e^{j\omega/M}) \\ &\quad\approx \Big[e^{-jN_d\omega} - H_k'(e^{j(\omega-2\pi k)/M}) \\ &\qquad - H_k'(e^{j(\omega-2\pi(k+1))/M})\Big] X_k(e^{j\omega/M}). \end{aligned} \tag{15}$$

With $X_k(e^{j\omega}) = H_k(e^{j\omega})X(e^{j\omega})$, $X_k^n(e^{j\omega})$ at the three subintervals, $\Omega_1' = \{\omega | k\pi \le \omega < k\pi + \omega_\delta'\}$, $\Omega_2' = \{\omega | k\pi + \omega_\delta' \le \omega < (k+1)\pi - \omega_\delta'\}$, and $\Omega_3' = \{\omega | (k+1)\pi - \omega_\delta' \le \omega \le (k+1)\pi\}$, i.e., $\bigcup_{i=1}^{3} \Omega_i' = \{\omega | k\pi \le \omega \le (k+1)\pi\}$, is given as (16) at the bottom of the page, which is shown in Fig. 6(c). This analysis is also applied to $D_k^n(e^{j\omega})$ as shown in Fig. 4, and thus $D_k^n(e^{j\omega})$ is given as (17), shown at the bottom of the page. If $X_k^n(e^{j\omega})$ and $D_k^n(e^{j\omega})$ are used for adaptive filtering in subbands instead of $X_k^d(e^{j\omega})$ and $D_k^d(e^{j\omega})$ in the kth subband, the output of the adaptive filter $E_k(e^{j\omega})$ is given as (18), shown at the bottom of the page. This is not the case as in (4) and (6) where $G_k(e^{j\omega})$ has to match the desired $H(e^{j\omega/M})$ while simultaneously matching the aliased responses $H(e^{j(\omega-2\pi k)/M})$ at $\omega \in \Omega_1$ and $H(e^{j(\omega-2\pi(k+1))/M})$ at $\omega \in \Omega_3$ in order to make $\left|E_k(e^{j\omega})\right|$ zero. From (18), $G_k(e^{j\omega})$ needs to match just the desired response $H(e^{j\omega/M})$ to make $\left|E_k(e^{j\omega})\right|$ zero. Therefore, the interband aliasing error can be made to be almost zero.

IV. Improvement of Spectral Flatness of Alias-Free Subband Signals

As shown in Fig. 6(c), $X_k^n(e^{j\omega})$ has spectral dips at the subintervals Ω_1' and Ω_3' and so does $D_k^n(e^{j\omega})$. The size of the spectral dips depends on the design of $H_k'(e^{j\omega})$. A poor design of $H_k'(e^{j\omega})$ can reduce the spectral flatness and thus reduce the convergence rate. The spectral dips at Ω_1' and Ω_3' can be reduced by using a minimum-phase filter $W(e^{j\omega})$ that has the following ideal magnitude response

$$|W(e^{j\omega})| = \begin{cases} \frac{1}{|e^{-jN_d\omega} - H_k'(e^{j(\omega-2\pi k)/M})|}, & \omega \in \Omega_1', \\ 1, & \omega \in \Omega_2', \\ \frac{1}{|e^{-jN_d\omega} - H_k'(e^{j(\omega-2\pi(k+1))/M})|}, & \omega \in \Omega_3'. \end{cases} \quad (19)$$

This is shown in Fig. 6(d). $W(e^{j\omega})$ can be designed to be of lower order than that of $H_k'(e^{j\omega})$, since it has a transition bandwidth that is M times wider than $H_k'(e^{j\omega})$. The design procedure of $W(e^{j\omega})$ is as follows: first, we design a minimum-phase bandpass filter with passband Ω_2' and transition bands Ω_1' and Ω_3'. The designed minimum-phase bandpass filter is inverted to give $W(e^{j\omega})$, and thus $W(e^{j\omega})$ is designed to be a minimum-phase filter.

The output of $W(e^{j\omega})$ in the kth subband $X_k^w(e^{j\omega})$ shown in Fig. 6(e) is given as

$$X_k^w(e^{j\omega}) = W(e^{j\omega})X_k^n(e^{j\omega}). \quad (20)$$

The kth desired signal $D_k^w(e^{j\omega})$ is obtained using $W(e^{j\omega})$ in the same way as $X_k^w(e^{j\omega})$. Therefore, when $X_k^w(e^{j\omega})$ and $D_k^w(e^{j\omega})$ are used for adaptive filtering in subbands instead of $X_k^d(e^{j\omega})$ and $D_k^d(e^{j\omega})$ in the kth subband, $E_k^w(e^{j\omega})$ is given as (21), shown at the bottom of the page. As represented in (21), the kth adaptive filter $G_k(e^{j\omega})$ needs to match only $H(e^{j\omega/M})$ as in (18) achieving the spectral flatness. The output of the

$$M \cdot X_k^n(e^{j\omega}) \approx \begin{cases} \left[e^{-jN_d\omega} - H_k'(e^{j(\omega-2\pi k)/M})\right] H_k(e^{j\omega/M})X(e^{j\omega/M}), & \omega \in \Omega_1', \\ e^{-jN_d\omega}H_k(e^{j\omega/M})X(e^{j\omega/M}), & \omega \in \Omega_2', \\ \left[e^{-jN_d\omega} - H_k'(e^{j(\omega-2\pi(k+1))/M})\right] H_k(e^{j\omega/M})X(e^{j\omega/M}), & \omega \in \Omega_3', \end{cases} \quad (16)$$

$$M \cdot D_k^n(e^{j\omega}) \approx \begin{cases} \left[e^{-jN_d\omega} - H_k'(e^{j(\omega-2\pi k)/M})\right] H_k(e^{j\omega/M})H(e^{j\omega/M})X(e^{j\omega/M}), & \omega \in \Omega_1', \\ e^{-jN_d\omega}H_k(e^{j\omega/M})H(e^{j\omega/M})X(e^{j\omega/M}), & \omega \in \Omega_2', \\ \left[e^{-jN_d\omega} - H_k'(e^{j(\omega-2\pi(k+1))/M})\right] H_k(e^{j\omega/M})H(e^{j\omega/M})X(e^{j\omega/M}), & \omega \in \Omega_3'. \end{cases} \quad (17)$$

$$M \cdot E_k(e^{j\omega}) \approx \begin{cases} \left[H(e^{j\omega/M}) - G_k(e^{j\omega})\right] \left[e^{-jN_d\omega} - H_k'(e^{j(\omega-2\pi k)/M})\right] H_k(e^{j\omega/M})X(e^{j\omega/M}), & \omega \in \Omega_1', \\ \left[H(e^{j\omega/M}) - G_k(e^{j\omega})\right] e^{-jN_d\omega}H_k(e^{j\omega/M})X(e^{j\omega/M}), & \omega \in \Omega_2', \\ \left[H(e^{j\omega/M}) - G_k(e^{j\omega})\right] \left[e^{-jN_d\omega} - H_k'(e^{j(\omega-2\pi(k+1))/M})\right] H_k(e^{j\omega/M})X(e^{j\omega/M}), & \omega \in \Omega_3'. \end{cases} \quad (18)$$

$$M \cdot E_k^w(e^{j\omega}) \approx \begin{cases} \left[H(e^{j\omega/M}) - G_k(e^{j\omega})\right] \left[e^{-jN_d\omega} - H_k'(e^{j(\omega-2\pi k)/M})\right] H_k(e^{j\omega/M})X(e^{j\omega/M})W(e^{j\omega}), & \omega \in \Omega_1', \\ \left[H(e^{j\omega/M}) - G_k(e^{j\omega})\right] e^{-jN_d\omega}H_k(e^{j\omega/M})X(e^{j\omega/M})W(e^{j\omega}), & \omega \in \Omega_2', \\ \left[H(e^{j\omega/M}) - G_k(e^{j\omega})\right] \left[e^{-jN_d\omega} - H_k'(e^{j(\omega-2\pi(k+1))/M})\right] H_k(e^{j\omega/M})X(e^{j\omega/M})W(e^{j\omega}), & \omega \in \Omega_3'. \end{cases} \quad (21)$$

adaptive filter $E_k(e^{j\omega})$ is obtained by passing $E_k^w(e^{j\omega})$ through $1/W(e^{j\omega})$ to negate the effect of $W(e^{j\omega})$. Since $W(z)$ is designed to be a minimum-phase filter, $1/W(z)$ is implemented by inverting $W(z)$.

V. Design of Bandwidth-Increased Analysis Filter Bank

In this section, the design procedure of the bandwidth-increased analysis filters is introduced. The bandwidth-increased analysis filters are used to extract the interband aliasing components from $X_k^s(e^{j\omega})$ of (9) as shown in Fig. 5. To achieve this, the kth bandwidth-increased analysis filters should satisfy the following conditions: the magnitude response of the kth bandwidth-increased analysis filter should be close to one and the phase response be linear in the frequency interval of $k\pi/M \le \omega \le (k+1)\pi/M$ for $k = 0, 1, \ldots, M-1$.

Before the design procedure is introduced, the design procedure of FIR cosine-modulated filter bank (CMFB) in [12] is summarized since the bandwidth-increased analysis filters can be designed by cosine modulation of the prototype filter. The analysis and synthesis filters of the CMFB are obtained by cosine modulation of the prototype linear-phase lowpass filter. If $p[n]$ is the impulse response of the FIR prototype filter, the impulse responses of the kth analysis and synthesis filters, $h_k[n]$ and $f_k[n]$, are given respectively as follows:

$$h_k[n] = 2p[n]\cos\left(\frac{\pi}{M}(k+0.5)\left(n-\frac{L}{2}\right)+\theta_k\right) \quad (22)$$

$$f_k[n] = 2p[n]\cos\left(\frac{\pi}{M}(k+0.5)\left(n-\frac{L}{2}\right)-\theta_k\right) \quad (23)$$

where L is the order of the FIR prototype filter, and $\theta_k = (-1)^k(\pi/4)$ for $k = 0, 1, \ldots, M-1$ [12]. The term θ_k on the right-hand side of (22) and (23) is used to cancel the interband aliasing component at the output of the filter bank and significant distortion around the frequencies $\omega = 0$ and $\omega = \pi$, respectively to obtain PR. However, the bandwidth-increased analysis filter bank does not need the PR condition, thus θ_k is discarded here. Therefore, if $p'[n]$ is the impulse response of the linear-phase FIR bandwidth-increased prototype filter, the impulse response of the kth bandwidth-increased analysis filter $h'_k[n]$ is given as follows:

$$h'_k[n] = 2p'[n]\cos\left(\frac{\pi}{M}(k+0.5)\left(n-\frac{L'}{2}\right)\right) \quad (24)$$

where L' is the order of the FIR bandwidth-increased prototype filter for $k = 0, 1, \ldots, M-1$. In order to design the magnitude response of the kth bandwidth-increased analysis filter to be unit from $k\pi/M$ to $(k+1)\pi/M$, the magnitude response of the prototype lowpass filter should be unit from 0 to $\pi/(2M)$. Such condition on the magnitude response of the prototype filter causes amplitude distortion to $H'_0(e^{j\omega})$ around $\omega = 0$ and to $H'_{M-1}(e^{j\omega})$ around $\omega = \pi$ but no amplitude distortion for $k = 1, \ldots, M-2$, as shown in Fig. 7 in the eight-channel case. Since the interband aliasing component exists only around $\omega = \pi/M$ in case of $X_0^s(e^{j\omega})$ and around $\omega = (M-1)\pi/M$ in case of $X_{M-1}^s(e^{j\omega})$, the amplitude distortions of the first and the last subband bandwidth-increased analysis filters do not affect the amplitude response of $X_0^b(e^{j\omega})$ and $X_{M-1}^b(e^{j\omega})$, if the following condition is satisfied,

$$\omega'_\delta \le \pi - \omega_\delta \quad (25)$$

where ω'_δ/M is the transition bandwidth of the prototype filter $H'(e^{j\omega})$ and ω_δ/M is that of the prototype filter of the filter bank. For example, when $k = 0$, the interband aliasing exists only around $\omega = (k+1)\pi/M = \pi/M$, and the spectral bump of $H'_0(e^{j\omega})$ exists around $\omega = 0$. Therefore, if the constraint (25) is satisfied, the interband aliasing and the spectral bump do not overlap with each other. The same analysis can be applied to the case of $k = M-1$. For $M = 2, 4, 8$, and 16, the stopband attenuations δ'_s, the normalized transition bandwidths ω'_δ/M, the orders L' of the designed prototype filters are given in Table I.

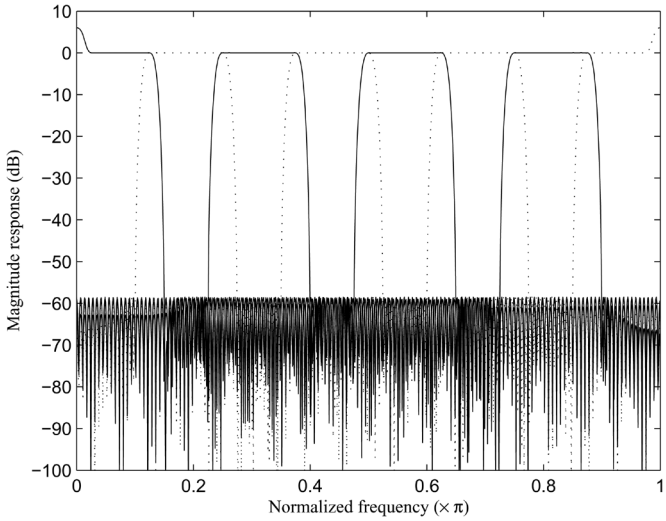

Fig. 7. Magnitude response of the eight-channel bandwidth-increased analysis filters.

TABLE I
Performances and the Orders of the Bandwidth-Increased Analysis Filters

M	δ'_s (dB)	ω'_δ/M ($\times\pi$)	L'
2	-58.5	0.1000	72
4	-58.5	0.0500	144
8	-58.5	0.0250	288
16	-58.0	0.0125	576

VI. Computational Complexity

One of the main benefits of using an SAF structure is the reduction in computational complexity gained over that of the fullband adaptive filtering when the unidentified system is of high order. In this section, the computational complexity of the proposed alias-free SAF algorithm is calculated in terms of the number of multiplications per sample (MPS) and compared to that of the fullband adaptive algorithm.

Fig. 4 shows the proposed alias-free SAF structure in the kth subband. The input and the desired signal are decomposed into a number of the subband signals using the analysis filter bank, and the interband aliasing is extracted and then subtracted from

each subband signal using bandwidth-increased analysis filters. The spectral dips of the subband signals are reduced, and the adaptive filtering is performed on each subband. The error in each subband is combined into an output error by the synthesis filter bank.

In the proposed SAF structure, the adaptive filtering in subbands based on the normalized LMS (NLMS) approximately requires $2N_a$ multiplications plus M divides for M samples for the filtering and adaptation, and thus $2N_a/M$ MPS plus one divide per unit, where N_a is the order of the system to be identified; however, since one divide is negligible compared to $2N_a/M$ multiplications, it will not be considered. The bandwidth-increased analysis filtering requires totally $2(L'+1)$ MPS since the input signal is not common to all the bandwidth-increased analysis filters $H'_k(z)$ for $k = 0, 1, \ldots, M-1$ in contrast to the case of the filter bank. Reducing the spectral dips and inverse filtering after adaptation also require totally about $3(L_w+1)$ MPS where L_w is the order of the filter for flattening the spectrum. If the implementation of the filter bank requires L_{FB} MPS, the overall MPS required by the proposed alias-free SAF structure is given as

$$\frac{2N_a}{M} + 2(L'+1) + 3(L_w+1) + L_{\mathrm{FB}}. \tag{26}$$

In this paper, a PR FIR CMFB proposed in [13] was used to analyze and synthesize the signals. The filter bank can be efficiently implemented by cosine modulation of an FIR prototype filter, and the FIR prototype filter can also be implemented efficiently using the two-channel cascaded lattice structure shown in [12]. When the order of the prototype filter is L, each lattice requires $2(2m+1)$ multiplications, where $m = (L+1)/(2M)$ is the order of the lattice. Since M lattice structures are required to implement the prototype filter and the each lattice operates at M-downsampled input rate, $3 \times 2(2m+1) = 6(L+1)/M+6$ MPS is required for the analysis filtering of the input and desired signals and the synthesis filtering of the output signal. In addition, the analysis of the input and the desired signal and the synthesis of the output requires $3\log_2 M$ MPS of three discrete cosine transform (DCT) for cosine modulation. Therefore, if the above computational complexity is substituted for L_{FB}, the overall MPS is given as

$$\frac{2N_a}{M} + 2(L'+1) + 3(L_w+1) + 6\left(\frac{(L+1)}{M}+1\right) + 3\log_2 M. \tag{27}$$

The first term corresponds to the filtering and adaptation of the adaptive filters in subbands, the second term corresponds to the filtering of the bandwidth-increased analysis filters, the third term corresponds to filterings for the spectral flatness, the fourth term corresponds to the implementation of the prototype filter, and the last term corresponds to the computation of three discrete cosine transforms (DCT) for cosine modulation. When the order of the system to be identified N_a is high, the overall MPS is approximated as $2N_a/M$, which is M times smaller than $2N_a$ MPS of the fullband NLMS algorithm. Since the transition bandwidth of the bandwidth-increased analysis filter $H'_k(z)$ needs to be designed to be narrower as the number of the subbands increases, the order of the bandwidth-increased filter H'_k, L', increases. Therefore, the total MPS can be approximated as

$$\frac{2N_a}{M} + 2L'. \tag{28}$$

However, since the order of the bandwidth-increased FIR analysis filter is generally smaller than that of the system to be identified, the proposed SAF structure still requires smaller computational load than the fullband structure.

TABLE II
PERFORMANCES AND THE ORDERS OF THE FIR PROTOTYPE FILTERS

M	δ_s (dB)	ω_δ/M ($\times\pi$)	L
2	-62	0.210	40
4	-59	0.121	80
8	-58	0.057	128
16	-59	0.032	256

VII. SIMULATIONS

By computer simulation, the convergence behavior of the proposed SAF algorithm that is almost alias-free was compared to those of the fullband NLMS and the conventional SAF algorithms in [3], [6], [10]. The simulations using the proposed SAF algorithm were performed by varying the number of subbands, that is, for $M = 2$, 4, 8, and 16. The stopband attenuations δ_s, the normalized transition bandwidths ω_δ/M, the orders L of the prototype filters of the PR FIR CMFBs are described in Table II. All the FIR CMFBs incorporated in the proposed structure had similar stopband attenuations around -60 dB, and their transition bandwidths were decreased as the number of the subbands increased. The bandwidth-increased analysis filters that were presented in Table I were used for extracting the interband aliasing. The filter $W(z)$ with order 14 was used for all cases of the simulations.

Four simulation experiments were conducted each with a different input: a white noise input of unit variance, a colored input, and a speech input.

A. White Noise Input

The proposed SAF with critical sampling and the fullband NLMS algorithms were evaluated using a white noise input of length 60000 with unit variance. The order of the FIR system to be identified was 1999. The normalized step-size of the NLMS algorithm was set to a value of 0.5 for all experiments. The simulations using the proposed SAF were conducted by varying the number of subbands, that is, for $M = 2$, 4, 8, and 16. All the orders of the adaptive filters in each subband were set to $\lceil 1999/M \rceil$ where $\lceil x \rceil$ represents the nearest integer of x towards infinity. A white Gaussian noise of variance 10^{-7} was added to the desired signal as a measurement noise. The MSE evolutions of the proposed SAF and the fullband NLMS algorithm are shown in Fig. 8.

The figure shows that the convergence rates of both the proposed SAF and the fullband NLMS algorithms were similar for a white noise input; however, the fullband reached lower steady-state MSE than the proposed after convergence. The steady-state MSE of the fullband is determined by the noise power (10^{-7}).

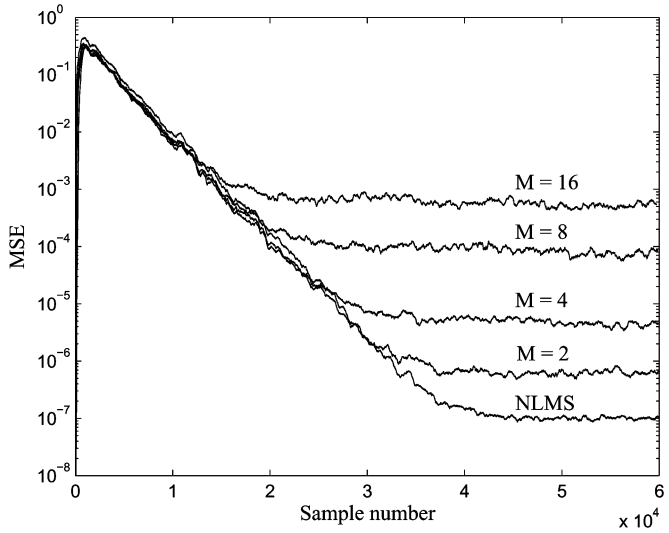

Fig. 8. MSE performance for the proposed SAF algorithm for different values of M and the fullband NLMS algorithm for a white noise input.

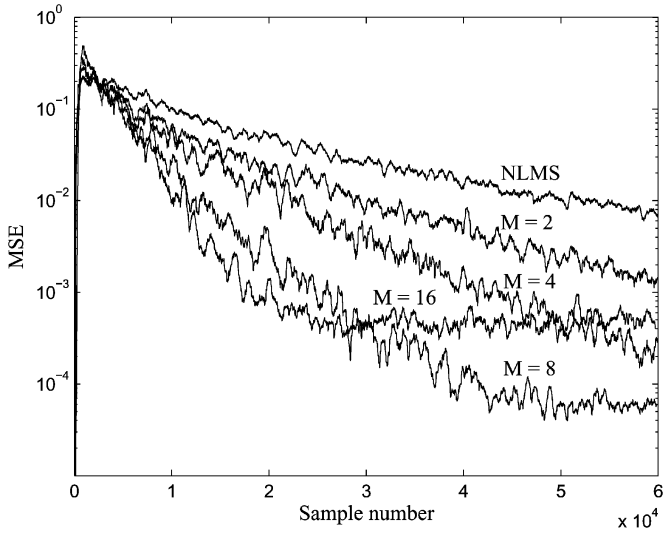

Fig. 9. MSE performance for the proposed SAF algorithm for different values of M and the fullband NLMS algorithm for a colored input.

Although the steady-state MSE of the proposed depends on the noise power, it depends more on the stopband attenuation of the filter banks and the number of the subbands for noise level comparable to or less than the stopband attenuation. The aliasing due to the nonzero stopband attenuation of the filter banks after downsampling increases as the number of subbands increases, and the aliasing still remains as error after convergence. This increases the steady-state MSE of the proposed SAF, and thus the steady-state MSE of the proposed increases with increase in the number of subbands. This is a disadvantage observed in all SAF algorithms, unless the algorithm eliminates the aliasing perfectly.

B. Colored Input

The simulation using a colored input was conducted. The simulation conditions were similar to those when using white noise. The colored input was generated by passing the white noise of unit variance through a first-order IIR filter with a pole location at $z = 0.9$ and then normalized to have unit variance. The MSE evolution is shown in Fig. 9.

Under this condition, the proposed SAF algorithm performed better than the fullband NLMS algorithm. Increasing the number of subbands led to better convergence rate, but larger MSE after convergence. When the number of subbands is 16, the convergence rate was similar to that when using white noise input. The MSE after convergence is also determined by the characteristics of the filter banks and the number of the subbands as in the case of white noise input.

C. Speech

An acoustic echo cancellation (AEC) experiment was conducted with real speech sampled at 8 kHz. The length of a room impulse response to be identified was 2000. The residual echoes using the proposed eight-channel SAF algorithm and the fullband NLMS algorithm are shown in Fig. 10.

It shows the proposed SAF algorithm cancelled the echo better than the fullband NLMS algorithm under this condition.

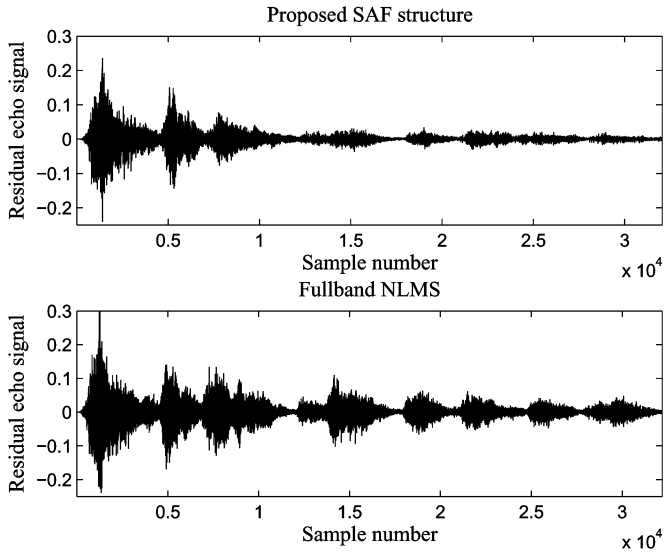

Fig. 10. Residual echo signals using the proposed eight-channel alias-free SAF algorithm and the fullband NLMS algorithm for speech input.

D. Comparison of Performances

The performance of the proposed SAF algorithm was compared to those of the SAF algorithms proposed in [3], [6], [10], when $M = 4$. The order of the FIR system to be identified was 1959. For a fair comparison, the order of the adaptive filters in the subbands for all algorithms was set to 500. All algorithms other than the SAF based on sparse subfilters in [10] require a minimum of order 490. The computational complexity of the SAF algorithms for each M is given in Table III. In the proposed algorithm, the computational complexity depends on a number of the factors that include the length of the bandwidth-increased analysis filters. Depending on how you design the bandwidth-increased analysis filters, there is a tradeoff between the computational complexity and the performance. Using a simple linear-phase FIR filter, the computation complexity shown in Table III is obtained. When M is equal to or greater than 16, the SAF

TABLE III
COMPUTATIONAL COMPLEXITY OF THE SAF ALGORITHMS FOR SEVERAL VALUES OF M, WHEN $N_a = 1959$

SAF	Complexity (MPS)	M			
		2	4	8	16
Proposed	$2N_a/M + 2L'$	2100	1270	1070	1400
Non-overlapping [3]	$2N_a/M$	1960	980	490	240
Auxiliary subband [6]	$2N_a$	3920	3920	3920	3920
Sparse subfilters [10]	$6N_a/M$	5880	2940	1470	730

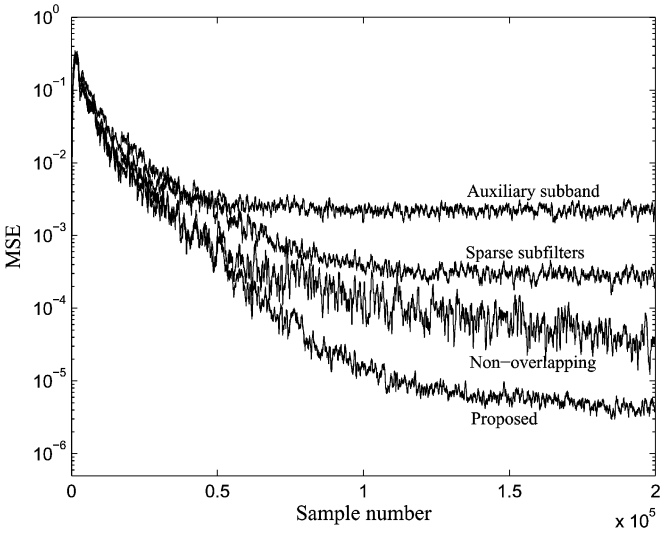

Fig. 11. Comparison of the performances of the proposed alias-free SAF algorithm and the conventional SAF algorithms for a colored input when $M = 4$.

algorithm in [10] requires less computational complexity than the proposed. The SAF algorithm in [6] used the long adaptive filters in the auxiliary subbands, whose length is same to that of the adaptive filters in the main subbands.

As stated in Section VII-A, the steady-state MSE of almost all SAF including the proposed depends on the stopband attenuation of the filter banks and also on the number of subbands. In our simulations, the number of the subbands was set to 4, and the stopband attenuation of the filter banks was set to about -60 dB. The SAF in [10] uses two cascaded analysis filters in contrast to the other algorithms, so the stopband attenuation of the analysis filters is doubled. For a fair comparison, the SAF in [10] was evaluated using the cascaded analysis filters, whose combined stopband attenuation is same as that of the analysis filters of the other algorithms compared. So, the SAF in [10] used the cascaded analysis filters of the four-channel PR FIR analysis CMFB with 39 order and -32 dB stopband attenuation. The SAF algorithms in [3], [6] used the two-channel nonoverlapping filter bank with 40 order and -60 dB stopband attenuation, which are similar as those of the two-channel PR FIR CMFB. Using a tree structure, four-channel SAF structures were implemented [14]. The SAF algorithm in [6] used the auxiliary subband where the analysis filter of length 81 was used and the total length of all the adaptive filters was 2000. For a colored noise of length 200000, simulation result shown in Fig. 11 was obtained.

Under this condition, the proposed SAF achieved faster convergence rate and lower MSE than the other algorithms. If we wait long enough, the SAF using the nonoverlapping filter bank achieves the steady-state MSE close to that of the proposed SAF. As stated in Section I, the SAF using the nonoverlapping filter bank introduces large spectral gaps at the output, especially as the number of the subbands increases. The SAF in [10] achieved the MSE around -36 dB, which is approximately a half of the stopband attenuation of the cascaded analysis filters. The SAF using the auxiliary subband had larger MSE in the auxiliary subbands than in the main subbands, even when the long adaptive filters in the auxiliary subbands were used. So, it had larger MSE at the output than the other algorithms.

VIII. CONCLUSION

In this paper, in order to fully exploit the benefits of SAF, a structure with critical sampling that is virtually alias-free is proposed. The interband aliasing is extracted in each subband using the bandwidth-increased FIR linear-phase analysis filters and then subtracted from each subband signal. The use of the bandwidth-increased analysis filters introduces an extra computational load. The almost alias-free subband signals have the spectral dips, so the spectral dips are reduced using a filter for the spectral flatness and then the outputs are used for adaptive filtering in each subband. The computational complexity of the proposed SAF algorithm is approximately reduced by M compared to that of the fullband algorithm. Simulations results show that the proposed subband structure achieves similar convergence rate to the fullband structure for white noise input and better convergence rate than both the equivalent fullband at lower computational complexity and the conventional SAF structures for colored input.

REFERENCES

[1] S. Haykin, *Adaptive Filter Theory*. Englewood Cliffs, NJ: Prentice-Hall, 1996.
[2] D. R. Morgan, "Slow asymptotic convergence of LMS acoustic echo cancelers," *IEEE Trans. Speech Audio Process.*, vol. 3, no. 2, pp. 126–136, Mar. 1995.
[3] H. Yasukawa, S. Shimada, and I. Furukawa, "Acoustic echo canceller with high speech quality," in *Proc. IEEE Int. Conf. Acoust., Speech, Signal Process.*, Dallas, TX, Apr. 1987, pp. 2125–2128.
[4] A. Gilloire and M. Vetterli, "Adaptive filtering in subbands," in *Proc. IEEE Int. Conf. Acoust., Speech, Signal Process.*, Apr. 1988, pp. 1572–1575.
[5] A. Gilloire and M. Vetterli, "Adaptive filtering in subbands with critical sampling: analysis, experiments, and application to acoustic echo cancellation," *IEEE Trans. Signal Process.*, vol. 40, no. 8, pp. 1862–1875, Aug. 1992.
[6] V. S. Somayazulu, S. K. Mitra, and J. J. Shynk, "Adaptive line enhancement using multirate techniques," in *Proc. IEEE Int. Conf. Acoust., Speech, Signal Process.*, Glasgow, U.K., May 1989, pp. 928–931.
[7] W. Kellermann, "Analysis and design of multirate systems for cancellation of acoustic echoes," in *Proc. IEEE Int. Conf. Acoust., Speech, Signal Process.*, Apr. 1988, pp. 2570–2573.
[8] M. Hartneck, S. Weiss, and R. W. Stewart, "Design of near perfect reconstruction oversampled filter banks for subband adaptive filters," *IEEE Trans. Circuits Syst. II*, vol. 46, no. 8, pp. 1081–1085, Aug. 1999.
[9] S. S. Pradhan and V. U. Reddy, "A new approach to subband adaptive filtering," *IEEE Trans. Signal Process.*, vol. 47, no. 8, pp. 655–664, Aug. 1999.
[10] M. R. Petraglia, R. G. Alves, and P. S. R. Diniz, "New structures for adaptive filtering in subbands with critical sampling," *IEEE Trans. Signal Process.*, vol. 48, no. 12, pp. 3316–3327, Dec. 2000.
[11] B. E. Usevitch and M. T. Orchard, "Adaptive filtering using filter banks," *IEEE Trans. Circuits Syst. II*, vol. 43, no. 3, pp. 255–265, Mar. 1996.

[12] P. P. Vaidyanathan, *Multirate Systems and Filterbanks*. Englewood Cliffs, NJ: Prentice-Hall, 1993.
[13] R. D. Koilpillai and P. P. Vaidyanathan, "Cosine-modulated FIR filter banks satisfying perfect reconstruction," *IEEE Trans. Signal Process.*, vol. 40, no. 4, pp. 770–783, Apr. 1992.
[14] S. K. Mitra, H. Babic, and V. S. Somayazulu, "A modified perfect reconstruction QMF bank with an auxiliary channel," in *Proc. IEEE Symp. Circuits Syst.*, Portland, OR, May 1989, pp. 2132–2135.

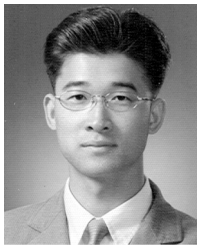

SangGyun Kim (S'02) received the B.S. and M.S. degrees in electrical engineering and computer science (EECS) from the Korea Advanced Institute of Science and Technology (KAIST), Daejeon, Korea, in 1999 and 2001, respectively. He is currently working towards the Ph.D. degree at the KAIST.

He joined the Multimedia Processing Laboratory in EECS at KAIST in 2001. His research interests include multirate signal processing, adaptive filtering, and blind source separation.

Mr. Kim is a student member of the Acoustical Society of Korea (ASK) and the Institute of Electrical Engineers of Korea (IEEK).

Chang D. Yoo (S'92–M'96) received the B.S. degree in engineering and applied science from the California Institute of Technology, Pasadena, in 1986, the M.S. degree in electrical engineering from Cornell University, Ithaca, NY, in 1988, and the Ph.D. degree in electrical engineering from the Massachusetts Institute of Technology (MIT), Cambridge, in 1996.

From January 1997 to March 1999 he worked at Korea Telecom as a Senior Researcher. He joined the Department of Electrical Engineering at the Korea Advanced Institute of Science and Technology (KAIST), Daejeon, Korea, in April 1999. From March 2005 to March 2006, he was with Research Laboratory of Electronics at MIT. His current research interests are in the application of machine learning and digital signal processing in multimedia.

Dr. Yoo is a member of Tau Beta Pi and Sigma Xi.

Truong Q. Nguyen (S'95–M'01–SM'95–F'05) received the B.S., M.S., and Ph.D. degrees in electrical engineering from the California Institute of Technology, Pasadena, in 1985, 1986, and 1989, respectively.

He was with the Massachusetts Institute of Technology (MIT) Lincoln Laboratory, Cambridge, from June 1989 to July 1994, as a Member of Technical Staff. During the academic year 1993–1994, he was a Visiting Lecturer at MIT and an Adjunct Professor at Northeastern University. From August 1994 to July 1998, he was with the Department of Electrical and Computer Engineering Department, University of Wisconsin, Madison. He was with Boston University from August 1996 to June 2001. He is currently a Professor at the Department of Electrical and Computer Engineering, University of California, San Diego (UCSD). His research interests are video processing algorithms and their efficient implementation. He is the coauthor (with Prof. G. Strang) of a popular textbook *Wavelets & Filter Banks* (Cambridge, MA: Wellesley-Cambridge Press, 1997), and the author of several Matlab-based toolboxes on image compression, electrocardiogram compression, and filter bank design. He has over 200 publications.

Prof. Nguyen received the IEEE TRANSACTIONS IN SIGNAL PROCESSING Paper Award (in the Image and Multidimensional Processing area) for the paper he coauthored with Prof. P. P. Vaidyanathan on linear-phase perfect-reconstruction filter banks in 1992. He received the NSF Career Award in 1995 and is currently the Series Editor (Digital Signal Processing) for Academic Press. He served as Associate Editor for the IEEE TRANSACTIONS ON SIGNAL PROCESSING from 1994 to 1996, for the IEEE TRANSACTIONS ON CIRCUITS & SYSTEMS from 1996 to 1997 and for the IEEE TRANSACTIONS ON IMAGE PROCESSING from 2004 to 2005.